Laurent Babout*, Marcin Janaszewski*

Analysis of Bridge Ligaments in 3D Volumetric Images Using Discrete Topology

1. Introduction

In the field of materials science, the last decade has known a constant increase of application of X-ray (micro)tomography to provide valuable volumetric information about microstructure and its evolution during special condition, such as special temperature conditions [5, 9], mechanical test or corrosion and environmental interactions [13]. The improvement of computational means and the flexibility of 3D data handling have also greatly facilitated the direct incorporation of volumetric data into 3D models [4]. One exemplary case that illustrates the strong interest in using X-ray (micro)tomography is the study of intergranular stress corrosion cracking in austenitic stainless steel. Recent work carried out at the ID-19 microtomography beamline at the European Synchrotron Radiation Facility (ESRF) has actually shown, for the first time in 3D, evidence of material ligament that bridges the crack path [2]. Recent study of King *et al.* [7] coupling X-ray microtomography with Diffraction Computed Tomography [10] has clearly demonstrated that most of these ligaments present special crystallographic orientation that are known to be resistant to cracking to a certain extent. However, their crystallographic study of bridges remained manual and revealed large uncertainty in the calculation of the bridge orientation, in respect with the loading axis.
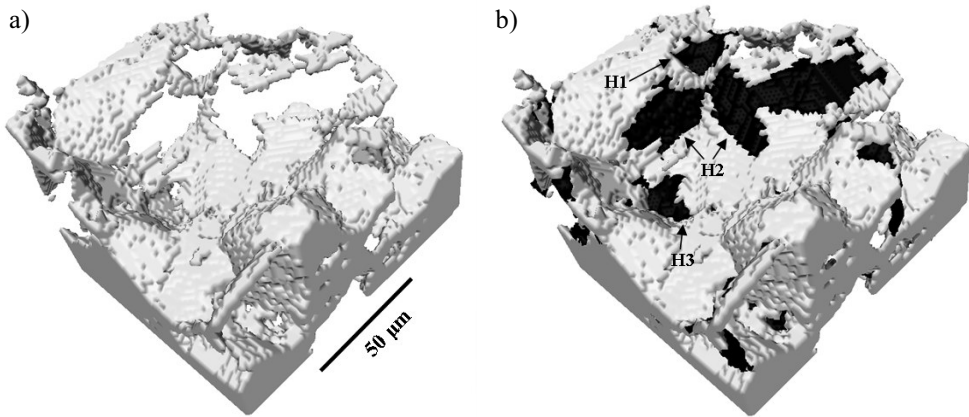
A quantitative analysis of the bridge ligament property needs a segmentation of these features which, for a topological point of view, correspond to holes. However, this segmentation cannot be approached with classical method based on connectivity or edge detection, since these holes do not correspond to a subset of the 3D space. Janaszewski *et al.* [6] recently proposed a modified version of the algorithm developed by [1]. This method takes into account the geometrical and topological characteristics of the feature corresponding to the crack in order to first, close, then fill holes, knowing the local thickness of the surrounding crack. An exemplar result of such approach that only considers hole closing is shown in Figure 1. One can see that the algorithm successfully close holes. However, one can discern a closed hole that actually corresponds to the connection of 2 possible bridge ligaments,

---

* Computer Engineering Department, Technical University of Lodz

via a thin isthmus. This junction is possible, in a microstructural point of view, since this isthmus can take place at a junction of multiple grain boundaries. However, it can also occur do to the possible dual effect of low resolution so that the crack is locally so thin to be resolved, resulting in such thin connection. A necessary step prior to analysing the features property and the final classification of holes as real bridge ligaments is to distinguish objects which potentially consist of several connected holes in order to separate them.

This paper presents a first approach to analyse holes and perform subsequent disconnection, based on topological considerations. The description of our method is preceded by a short introduction about some topological definitions. Before conclusion, a section presents and discusses the results of the algorithm applied to a 3D dataset corresponding to a stress corrosion crack in stainless steel.

Fig. 1. 3D rendering of crack with holes (a) only crack (light grey colour) (b) crack with hole closed (dark colour)

2. Qualitative description of holes

Figure 1 presents an example of ROI (Region Of Interest) that contains a couple of holes inside a feature that corresponds to a crack. According to the hole closing algorithm [6], all holes are 1 voxel thick. A qualitative analysis of hole geometry shows that they vary in shape. Some are consistent with the normal shape of bridge ligaments, i.e. lamellar- or triangular-type shapes (see holes noted H1 and H3 in Fig. 1b). Others are rather with a more irregular shape, as illustrated by the hole H2 in Figure 1b. However, a closer look at hole H2 reveals that the feature has a special topography, with areas with different normal orientation and convexity (see Fig. 2). The latter point is consistent with the fact that grains inside austenitic stainless steel may present non-planar faces. The boundary between these zones is at least composed of a single voxel and connects much larger features. The algorithm presented in this paper is a first approach to select and delete these isthmus-type boundaries in order to optimize the volumetric image analysis and classification of the holes as bridge ligaments.

Fig. 2. Zoomed view of hole H2 highlighting isthmuses with dashed lines.
Other portions of the hole encircled with dashed ellipses may also correspond
to boundaries but are not treated in this algorithm

3. Basic topological notions

In this section, we recall some basic topological notions for binary images, which are necessary to understand the sequel of the paper. A more extensive review is provided in [8].

We denote by Z the set of integers, by N the set of nonnegative integers, by N_+ the set of strictly positive integers and by R_+ the set of strictly positive real values. Moreover, assume that $E = Z^3$. A point $x \in E$ is defined by (x_1, x_2, x_3) with $x_i \in Z$. We consider the three neighbourhoods: N_6, N_{18}, N_{26} defined by, $\forall x \in E$:

$$N_6(x) = \{x' \in E; |x_1 - x'_1| + |x_2 - x'_2| + |x_3 - x'_3| \le 1\},\tag{1}$$

$$N_{18}(x) = \{x' \in E; |x_1 - x'_1| + |x_2 - x'_2| + |x_3 - x'_3| \le 2\} \cap N_{26}(x),\tag{2}$$

$$N_{26}(x) = \{x' \in E; Max[\,|x_1 - x'_1|, |x_2 - x'_2|, |x_3 - x'_3|] \le 1\}.\tag{3}$$

The set $N_n(x)$ is called the *n-neighbourhood* of x. We define $N^*_n(x) = N_n(x) \backslash \{x\}$, with $n = 6, 18, 26$. Any point y of $N^*_n(x)$ is said to be *n-adjacent* ($n = 6, 18, 26$) to x, we also say that y is an *n-neighbour* of x. An *n-path* π is a (possibly empty) sequence of points $x_0 \dots x_k$, with x_i *n*-adjacent to x_{i-1}, for $i = 1 \dots k$. If π is not empty, the length of π is equal to k. If $x_0 = x_k$, π is *closed*.

An object $X \in E$ is said to be *n-connected* if, for any two points of X, there is an *n*-path in X between these two points. The set composed of all the *n*-connected components of X is denoted $C_n(X)$. Note that, if X is finite, the infinite connected component of $\overline{X}$ is called the *background*, the other connected components of $\overline{X}$ are called the *cavities*. Moreover, if we use an *n*-connectivity for X we have to use another *m*-connectivity for $\overline{X}$, i.e., the 6-connectivity for X is associated to the 18- or the 26-connectivity for $\overline{X}$ (and vice versa). This is necessary for avoiding connectivity paradoxes [8]. It is sometimes useful to distinguish the

6-connectivity associated with the 18-connectivity and the 6-connectivity associated with the 26-connectivity. In order to handle his distinction, a 6_+-notion will indicate a 6-notion associated with the 18-connectivity. So we can have $(n; m)$ = (6; 26); (26; 6); (6+; 18) or (18; 6+).

Each point x of X can also be defined according to its topological characteristics [3]. Topological numbers for each point are based on the study of the corresponding *geodesic neighbourhood* which is linked to the n-connectivity of X. Bertrand *et al.* have defined mathematically different geodesic neighbourhoods $G_n(x, X)$ that can be summarised as follows. For $G_{6+}(x, X)$, $G_{16}(x, X)$ and $G_{26}(x, X)$, the neighbourhood is equivalent to $N^*_{26}(x) \cap X$, while $G_6(x, X)$ is equivalent to $N^*_{18}(x) \cap X$.

We can now give a definition of topological numbers [3]. Let $X \in E$ and $x \in E$, the two topological numbers are defined as follows (#X stands for the cardinality of X):
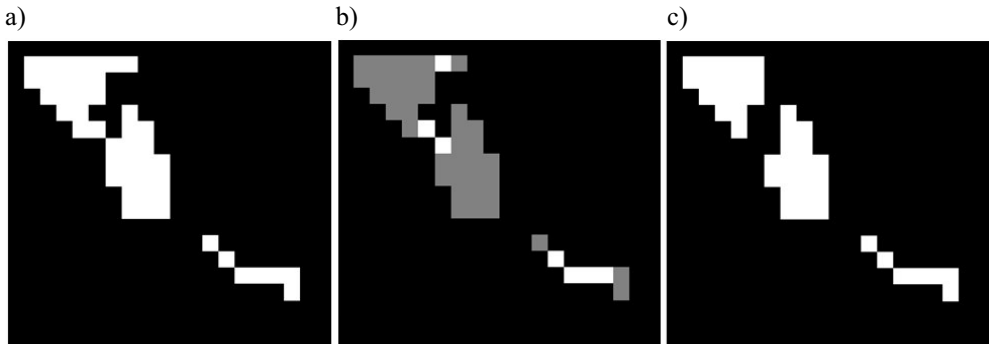
$$T_n(x, X) = \#C_n\big[G_n(x, X)\big]$$
$$T_m(x, \bar{X}) = \#C_m\big[G_m(x, \bar{X})\big] \tag{4}$$

The topological characteristic of a point can be done based on the defined above numbers. In particular, this notion is used to define points that compose a feature such as border, end-point, junctions or isthmus [11]. Points that characterise the latter case have $T_n(x, X) \geq 2$ and $T_m(x, \bar{X}) = 1$. This property will be used in the algorithm presented in the next section.

4. Feature disconnection algorithm

As we stated previously, our first approach only concentrates on the deletion of isthmus points, since a qualitative analysis of the holes revealed a significant amount of features that presented such special points (or voxels). In general, isthmus is seen as a thin zone that connects 2 larger components. However, this description, in a topological point of view, is not always true. This is, for instance, illustrated in Figure 3 that presents the central image of a 3D stack of 3 images, the first and last image corresponding only to background(black colour). If we assume a 26-connectivity, the 2 components contains isthmus points (or voxels), as shown in white in Figure 3b. Deletion of these isthmuses in both components do not preserve the topology. However, their deletion affects differently the features. The first one with an initial large size is transformed into 3 disconnected components, 2 of them being of large size and have a morphological meaning. However, in the case of the second feature, the deletion of isthmuses transforms it into 2 small components that do not share characteristics with the original object. From the image analysis point of view, this transformation is not acceptable and should be avoided. This is even of greater importance since bridge ligaments with a lamellar-type shape are known to exist. In order to avoid such isthmus deletion, a simple volume threshold is applied. Before isthmus deletion, only the features which are larger or equal than a threshold value V_{th} are post-processed.

This minimum volume is also considered during the isthmus deletion: if a feature X is separated into N n-connected components which all have a volume lower than V_{th}, the isthmus deletion is disregarded. Otherwise, all isthmuses are deleted, as well as the N' n-connected components ($N' < N$) that have a volume lower than V_{th}. With such consideration, the algorithm mainly preserves the topology of small objects compared to the threshold volume and only treat large ones, as illustrated in Figure 3c.

a)   b)   c)

Fig. 3. 2D image of a 3D input image showing 2 objects (a). Previous and next images in the stack are set to background; same cross-section showing isthmuses (white colour) (b); output image after application of algorithm ***DelIsthmus()*** with 26-connectivity for the foreground (c)

The algorithm is formulated with the following pseudo-code, assuming that an object X corresponds to 1 n-connected component:

DelIsthmus(Input: X, V_{th}, m, n; Output: Y)

1) Y ← X

2) Calculate $T_n(x, X)$ and $T_m(x, \overline{X})$ for all x ∈ X

3) If X contains isthmus(es)
4)   Delete isthmus(es) from Y
5)   Calculate $C_n(Y)$
6)   For each Y' in $C_n(Y)$ calculate $V_{Y'}$
7)   If ∃ Y' in $C_n(Y)$ such that $V_{Y'} \geq V_{th}$
8)   Delete each object Y' in $C_n(Y)$ such that $V_{Y'} < V_{th}$
9) Return Y

5. Application to holes in 3D crack

The algorithm presented above have been tested on a 3D binary image of holes detected inside a corrosion crack using the algorithm developed by Janaszewski *et al.* [6]. The volume is 350×350×200 voxels in size with a voxel size of 1.4 μm. The initial volume

contains 1435 holes that have been closed. The volume distribution of the holes is shown in Figure 4. More than 65% of the population has a size strictly smaller than 4 voxels and 80% of the remaining holes have a size smaller than 20 voxels. The maximum size is larger than 1000 voxels. To the author's point of view, there has not been any 3D quantitative analysis of bridge ligaments size. However, 2D quantitative analysis on fracture surface of austenitic stainless steel after stress corrosion cracking reveals that the 2 most common shape of bridge ligaments, i.e. lamellar and triangular, can have a size between 5 to 50 μm [12]. A reasonable value for the threshold volume V_{th} is therefore 4 voxels. Table 1 presents the summary results of the algorithm in terms of numerical fraction of holes that have been processed.
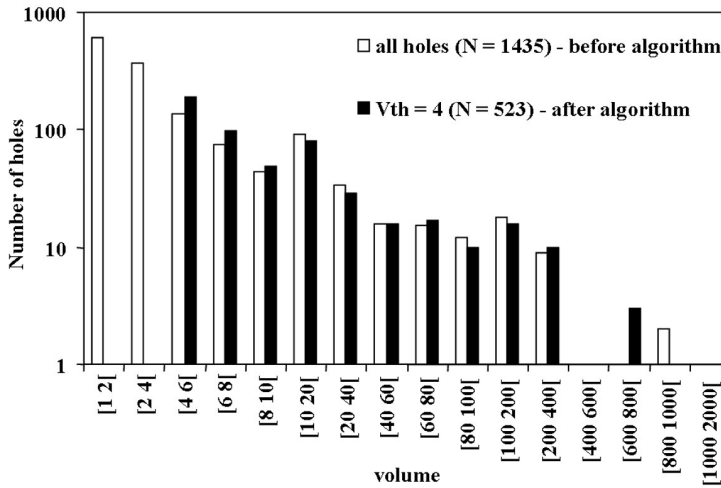

Fig. 4. Histogram of the size of all holes and those larger than 4 voxels, before and after algorithm computation, respectively

Three categories are taken into account:
– holes that does not present isthmus,
– holes with isthmus(es) but new components after isthmus deletion have their volume lower than V_{th},
– holes with isthmus(es) with at least one of the new components having a volume larger than V_{th}.

The table also displays the number of new holes that correspond to the division of each initial hole into at least 2 new components that satisfy $V \geq V_{th}$. One can see that the repartition between the 3 categories is relatively even when $V_{th} = 4$. The fraction of holes with isthmus treated larger than when all hole sizes are taken into account in the algorithm, the zero proportion of disregarded holes with isthmus(es) being valid since new components cannot have a size smaller than 1 voxel. Increasing the threshold volume to 8 also results in an increase of the fraction of treated holes with isthmus(es), and inversely in a decrease of non-treated holes. This is in agreement with the volume distribution presented in Figure 4
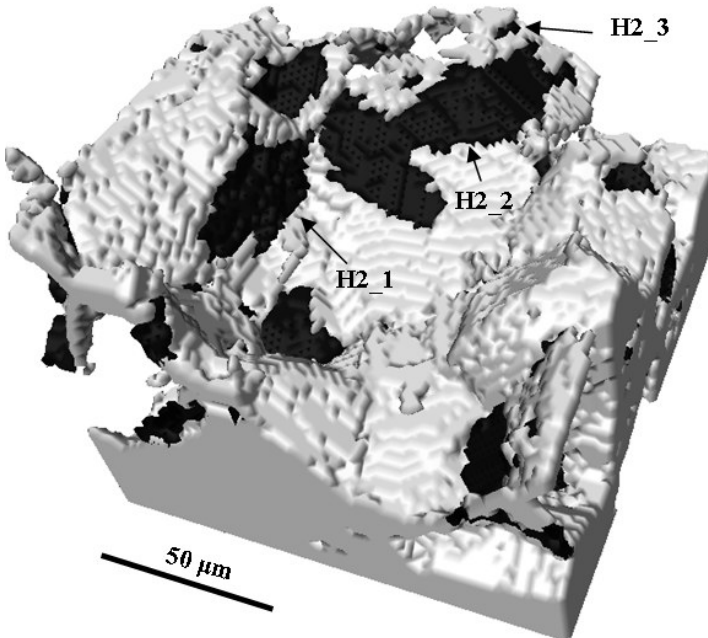
showing that a large fraction of new components larger than 4 voxels have a size smaller than 8 voxels. According to Table 1, the fraction of new holes is not negligible since it represents, for instance in the case of V_{th} = 4, around 15% of all holes and around 40% of the holes with isthmuses treated, the remaining 60% corresponds to cases where only one new component satisfies the volume criterion.

Table 1
Proportion of holes that are processed by the algorithm based on the presence on isthmuses.
N: number of initial holes. N': number of new holes

V_{th}	N	Holes with no isthmus (%)	Holes with isthmuses		
			Disregarded (%)	Treated (%)	N'
1	1435	74	0	26	584
4	455	31	31	38	68
8	245	24	29	47	29

Figure 5 shows the result of the algorithm on the portion of crack presented in Figure 1. The threshold volume was set to 4. One can see that the deletion of isthmuses on the hole that was presented in Figure 2 occurs at 2 places, resulting in the separation of the initial hole into 3 subsequent features

Fig. 5. 3D view of the crack and closed holes after application of the disconnection algorithm

The present method is worth of consideration, taking into account the relative large amount of connected holes via isthmus junction type. The algorithm especially works in the case where two or more holes with large size are connected via 1 voxel wide isthmus and can be seen as an alternative to classical watershed algorithm. However, the current algorithm has a limited application when isthmus is thicker, that I to say when the junction cross-section is more than 1 voxel. Moreover, the algorithm may result in a further wrong interpretation of the data when at least 2 holes of different geometrical characteristics, such as triangular and lamellar-type holes, by any chance, are connected. If the lamellar hole is locally 1 voxel wide, the algorithm will interpret this as isthmus and process unwanted isthmus deletion. More importantly, if the new labels are smaller in size than the threshold volume, they will be deleted as well. Modification of the algorithm to deal with both situations is currently under work.

6. Conclusion

The present paper has proposed a new algorithm, based on topological considerations to perform fragmentation of a cluster of holes that are connected via isthmus. The algorithm has been successfully applied, subsequently after hole closing algorithm, to a 3D dataset representing a stress corrosion crack in stainless steel that was obtained during X-ray microtomography experiment. Combined with the hole closing algorithm, this image processing algorithm will be an efficient tool to further characterise automatically 3D morphological and microstructural properties of bridge ligaments, especially if this is combined with data from Diffraction Computed Tomography. Work is in progress to extend the current approach to localize thicker junctions and perform new decision making about the fragmentation in new holes, depending on shape considerations.

Acknowledgments

References

[1] Aktouf Z., Bertrand G., Perroton L., *A three-dimensional holes closing algorithm.* Pattern Recognition Letters, t. 5, nr 23, 2002, 523–531.

[2] Babout L., Marrow T.J., Engelberg D., Withers P.J., *X-ray microtomographic observation of intergranular stress corrosion cracking in sensitised austenitic stainless steel.* Materials Science and Technology, nr 9, 2006, 1068–1075.

[3] Bertrand G., *Simple points, topological numbers and geodesic neighborhoods in cubic grids.* Pattern Recognition Letters, t. 10, nr 15, 1994, 1003–1011.

[4] Buffiere J.-Y., Cloetens P., Ludwig W., Maire E., Salvo L., *In situ X-ray tomography studies of microstructural evolution combined with 3D modeling.* MRS Bulletin, t. 6, nr 33, 2008, 611–619.

[5] Flin F., Brzoska J.-B., *The temperature-gradient metamorphism of snow: Vapour diffusion model and application to tomographic images.* Annals of Glaciology, nr 49, 2008, 17–21.

[6] Janaszewski M., Couprie M., Babout L., *Hole filling in 3D volumetric objects.* Pattern Recognition, 2009 Submitted.

[7] King A., Johnson G., Engelberg D., Ludwig W., Marrow J., *Observations of intergranular stress corrosion cracking in a grain-mapped polycrystal.* Science, t. 5887, nr 321, 2008, 382–385.

[8] Kong T.Y., Rosenfeld A., *Digital topology: Introduction and survey.* Computer Vision, Graphics, and Image Processing, t. 3, nr 48, 1989, 357–393.

[9] Limodin N., Salvo L., Boller E., Suéry M., Felberbaum M., Gailliègue S., Madi K., *In situ and real-time 3-D microtomography investigation of dendritic solidification in an Al-10 wt.% Cu alloy.* Acta Materialia, t. 7, nr 57, 2009, 2300–2310.

[10] Ludwig W., Schmidt S., Lauridsen E.M., Poulsen H.F., *X-ray diffraction contrast tomography: A novel technique for three-dimensional grain mapping of polycrystals. I. Direct beam case.* Journal of Applied Crystallography, t. 2, nr 41, 2008, 302–309.

[11] Malandain G., Bertrand G., Ayache N.: *Topological segmentation of discrete surfaces.* International Journal of Computer Vision, t. 2, nr 10, 1993, s. 183–197.

[12] Marrow T.J., Babout L., Jivkov A.P., Wood P., Engelberg D., Stevens N., Withers P.J., Newman R.C., *Three dimensional observations and modelling of intergranular stress corrosion cracking in austenitic stainless steel.* Journal of Nuclear Materials, t. 1–3, nr 352, 2006, 62–74.

[13] Stock S.R., *Recent advances in X-ray microtomography applied to materials.* International Materials Reviews, t. 3, nr 53, 2008, 129–181.